Preliminary evaluation of dual wavelength phased array imaging on neonatal brain function

Yu Chen
Departments of Biochemistry
    and Biophysics, and Bioengineering
University of Pennsylvania
Philadelphia, Pennsylvania 19104

Shuoming Zhou
Chunhua Xie
Shoko Nioka
Department of Biochemistry and Biophysics
University of Pennsylvania
Philadelphia, Pennsylvania 19104

Maria Delivoria-Papadopoulos
Endla Anday
Department of Pediatrics, Division of Neonatology
MCP Hahnemann University Hospital
Philadelphia, Pennsylvania 19132

Britton Chance
Department of Biochemistry and Biophysics
University of Pennsylvania
Philadelphia, Pennsylvania 19104

Abstract. Imaging of human tissue using noninvasive techniques has been of great interest in biomedical fields. Optical imaging has attracted a lot of attention because of its portability and economy. The possibility that a highly portable, fast, safe, and affordable imaging system which could obtain interpretable images of brain function for pre- and full-term neonates in a few seconds, has been explored in this article. We have used a sensitive optical topography system, termed phased array, in which a pair of equal-amplitude and antiphase light sources are applied to generate a sharp amplitude null and phase transition plane. This two-wavelength (750 and 830 nm), frequency encoded (50 and 52 MHz) phased array imaging system can indicate the blood concentration and oxygenation changes in blood model studies and during parietal brain activation in neonates. Significant functional responses, particularly to parietal stimulation in normal and pathological states of neonatal brain, have been revealed in our study. The preliminary clinical results are presented in this article. © 2000 Society of Photo-Optical Instrumentation Engineers.
[S1083-3668(00)01002-9]

1 Introduction

Noninvasive measurement of brain activity has been of increasing interest in recent years. Functional activation of the human brain is coupled to the localized changes in cerebral blood volume and oxygenation saturation.[1] Currently, positron emission tomography (PET) and functional magnetic resonance imaging (fMRI) are widely used to obtain images of brain activation related to various kinds of stimulation. Near-infrared imaging (NIRI) is a novel technique for measuring brain activity. Compared with PET and fMRI, NIRI has the advantages of portability, real-time measurement, and low cost.

Since Jobsis first showed that the absorption of hemoglobin could be observed in neonatal brain with near-infrared transillumination,[2] and Brazy et al. applied the optical method to monitor brain oxygenation levels of newborn infants,[3] much research work has been done in the area of noninvasive diagnosis of brain function by means of near-infrared spectroscopy (Chance et al.,[4] Hoshi et al.,[5] and Cope and Delpy[6]). Also, similar imaging of adults and neonates has been implemented by continuous light (Chance et al.[7]) and pulsed light (Hintz et al.[8]) successfully.

A previous study has shown that frequency modulated, single wavelength (780 nm) phase and amplitude cancellation method can be used for imaging sensorimotor and cognitive activation of adult and pre- and full-term neonate human brain function.[9] We have developed a two-wavelength (750 and 830 nm), 50 MHz phased array imaging (PAI) system for human brain function imaging. This system can provide information on blood concentration and oxygenation in a localized region. The preliminary application of the two wavelength phased array imaging (PAI) system of neonatal brain function due to parietal stimulation is presented here.

2 Theory

The basic geometry of a phased array unit is illustrated in Figure 1, where in-phase (0°) and antiphase (180°) sources $S1$ and $S2$ are equidistantly placed with respect to the photon detector D. In a homogeneous medium with optical absorption coefficient μ_a and reduced scattering coefficient μ_s', diffusion theory can be applied to describe the light propagation in tissue.[10]

In the situation of a sinusoidally intensity-modulated point source of light, we can obtain the frequency domain diffusion equation:[11]

$$[\nabla^2 + k^2]\Phi_{ac}(r,t) = -\frac{S_{ac}}{D}\delta(r), \tag{1}$$

where Φ is the photon density, D is the diffusion coefficient with $D = 1/3(\mu_a + \mu_s')$, and k is the complex wave number, $k^2 = (-v\mu_a + i\omega)/Dv$, here v is the speed of light in the medium. S_{ac} is the alternating-current (ac) component of source intensity. In our case, two antiphase sources are placed at $r = a$ and $r = -a$, so the diffusion equation can be written as:
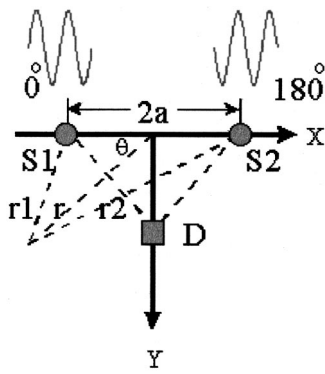
Fig. 1 Geometry for phased array unit. Two equal amplitude and antiphase (180° out-of-phase) sources are placed with a displacement of $2a$, and a detector is placed with equal distance to each source.

$$[\nabla^2+k^2]\Phi_{ac}(r,t)=-\frac{S1}{D}\delta(-a)+\frac{S2}{D}\delta(a), \quad (2)$$

where $S1$ and $S2$ are the ac intensities of two sources, respectively.

To illustrate the principle of phased array, we choose the simplest situation—infinite boundary condition. It is well known that the time-independent solution for Eq. (1) in an infinite-large scattering medium can be expressed as:[12]

$$U(r)=\frac{\nu S_{ac}}{4\pi Dr}\exp(ikr). \quad (3)$$

Since k is a complex number, Eq. (3) can be rewritten as

$$U(r)=\frac{\nu S_{ac}}{4\pi Dr}\exp(-k_r r)\exp(ik_i r), \quad (4)$$

where k_r is the real part of the wave number and k_i is the imaginary part, which corresponds to the phase shift produced by traveling in the scattering medium with respect to the source. The expressions for k_r and k_i are[12]

$$k_r=\left(\frac{\nu^2\mu_a^2+\omega^2}{D^2}\right)^{1/4}\cos\left(\frac{1}{2}\tan^{-1}\frac{\omega}{\nu\mu_a}\right), \quad (5)$$

$$k_i=\left(\frac{\nu^2\mu_a^2+\omega^2}{D^2}\right)^{1/4}\sin\left(\frac{1}{2}\tan^{-1}\frac{\omega}{\nu\mu_a}\right). \quad (6)$$

For a system with multiple sources, the total photon density, $U_t(r)$ can be obtained by superposition of individual sources, namely, $U_t(r)=\Sigma U_n(r)$. The phased array system consists of one in-phase (initial phase$=0°$) and one antiphase (initial phase$=180°$) source. As shown in Figure 1, the total photon density at position r is

$$U_t(r)=\frac{\nu S_{ac}}{4\pi D}\left[\frac{1}{r1}\exp(-k_r r1)\exp(ik_i r1)\right.$$
$$\left.+\frac{1}{r2}\exp(-k_r r2)\exp(ik_i r2+180°)\right], \quad (7)$$

where $r1$, $r2$, and r are related by

$$r1=\sqrt{a^2+r^2-2ar\cos\theta}, \quad (8)$$

$$r2=\sqrt{a^2+r^2+2ar\cos\theta}. \quad (9)$$

Figure 2 shows the cross-section of amplitude and phase profiles along a line parallel to X axis, which is simulating the coaxial scanning of the detector. The 10 cm region (from $x=-5$ cm to $x=+5$ cm) is discretized into 64 grids. The charts show that there is an amplitude null and phase transition of 180° in the middle plane across the midpoint between two sources, which agrees with previous simulation results by Kang et al.[13] When the detector is in the left side of both sources, it receives larger light signal from the left source ($S1$) than the right source ($S2$) since $S1$ has a shorter distance. This causes the phase signal to be predominated by $S1$. As the detector moves closer to $S1$, the amplitude increases and reaches the first peak. Then the amplitude decreases due to the increasing antiphase diffusing photon density wave from $S2$. It reaches a minimum when the detector is equidis-
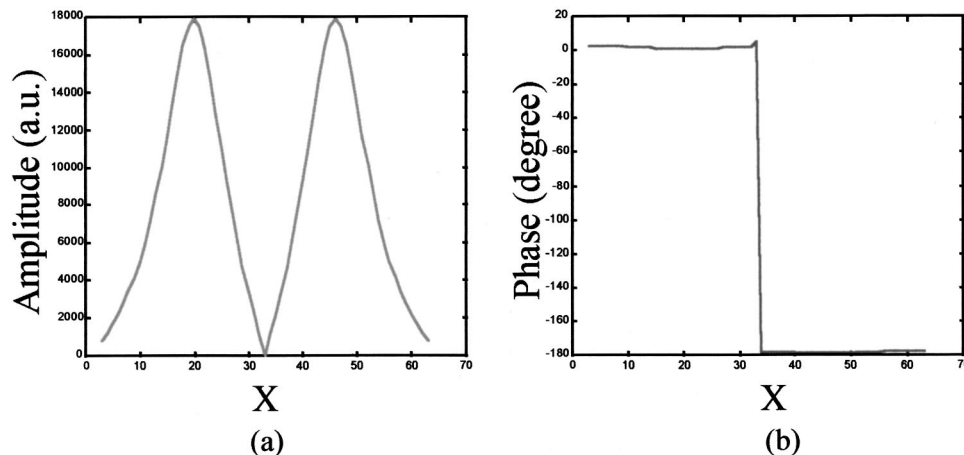
Fig. 2 The cross-section plot of amplitude (a) and phase (b) along a line parallel to X axis in Figure 1. (The number in abscissa means the grid index, with source position of $X=19$ and 45.)
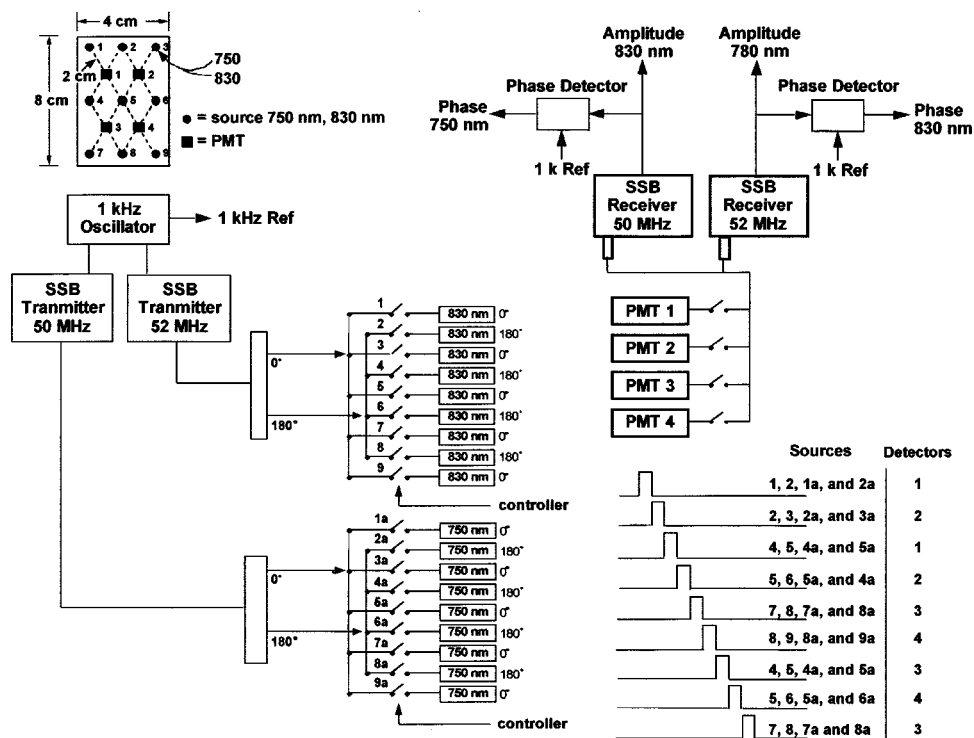
Fig. 3 Schematic of two-wavelength phased array imaging (PAI) system.

tant to both sources, then vise versa. The phase shows a sharp transition when the predominant source changed from $S1$ to $S2$. The numerical results illustrate that there forms a null plane through the midpoint of those two sources and perpendicular to the line connecting them. A small perturbation of absorption or scattering will sensitively alter the null plane, and cause an amplitude change and phase shift.[14]

3 System Description

3.1 Instrumentation

A schematic of our two-wavelength, phased array imaging system is illustrated in Figure 3. The system uses two different radio frequencies (50 and 52 MHz) to encode two wavelengths (750 and 830 nm), respectively. Both are modulated in the single side band (SSB) mode (1 kHz). The upper side band (USB) is chosen and split into 0° and 180° ±1° to achieve a sharp cancellation plane. There are nine laser diode sources (Sharp Corp., Japan) for each wavelength (total of 18) and four detector fiber bundles mounted on a 7 cm×4 cm rectangular rubber pad, with a source-detector separation of 2 cm. The fibers are then coupled into the R928 photomultiplier tubes (Hamamatsu Photonics, Japan). The output signals are sent to SSB receiver, which can detect the signal levels on the order of microvolts in a 2 kHz bandwidth,[9] and then decoded for each wavelength. The phase of the 1 kHz sine wave can be detected through a zero-crossing phase meter (Krohn-Hite Corp.) and the amplitude measurement is based on the automatic gain control (AGC) voltage. The combination of sources and detectors makes up 16 phase cancellation arrays in total. Examining the upper left inset in Figure 3, which

shows the sources and detectors configuration, each photomultiplier tube (PMT) has four sources around it, thus can form four phased array pairs. For example, for PMT No. 1, there are four pairs depending which two sources are chosen, i.e., source Nos. 1 and 2 consist one pair; source Nos. 1 and 4 form another; similarly source Nos. 2 and 5, as well as source Nos. 4 and 5. The detector is positioned appropriately to get an amplitude null and phase shift around 90°. A localized small change of absorption or scattering will cause significant perturbation in nearby phased array pairs and result in the phase shifts, which form the signals for imaging. The sampling time for each cycle is 16 s. The two-dimensional spatial resolution for this system is 1 cm and the signal to noise ratio is about 500 for a normal parietal response in 1 Hz bandwidth.[9]

3.2 Data Analysis

3.2.1 Signals in phased array

From the theoretical calculations shown in Figure 2, we learn that the amplitude signals are symmetric along the null plane. In other words, they are ambiguous, so that one cannot judge which side the object is in (left or right), while phase signal can differentiate the position information. This issue will be further discussed in the following model studies (part 4). For each wavelength, we record the phase shift ($\Delta\Phi$) in the unit of degree. In the two wavelength system, the wavelengths we chose are in different sides of the isosbestic point ($\sim$800 nm). For oxyhemoglobin, $\mu_a(750\,\text{nm}) < \mu_a(830\,\text{nm})$ while for deoxy-hemoglobin, $\mu_a(750\,\text{nm}) > \mu_a(830\,\text{nm})$, the difference of those two wavelengths can indicate the oxygenation/
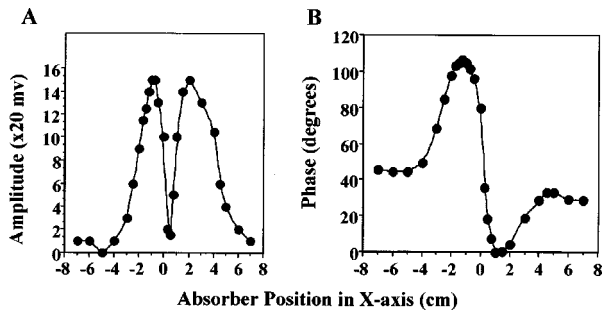
Fig. 4 Amplitude and phase transition with the displacement of absorber (source position: $X=\pm 2$ cm; absorber: black Delrin rod, 5 mm in diameter).

deoxygenation information. We take $|\Delta\Phi(830)| - |\Delta\Phi(750)|$, which can reveal oxygenation changes; and $\Delta\Phi(830)+\Delta\Phi(750)$, which can reveal the blood volume changes, as the signal for evaluation. For single wavelength (750 or 830 nm), the maximal phase shift is $\sim 90°$. In phased array image, for either oxygenation image or blood volume image, a typical response on adult brain is $\sim 50°$–$60°$. Since the blood volume image is the sum of changes in both wavelengths, the phase shift can exceed 90° in some circumstance. The total signal in phased array is defined as the sum of absolute values of oxygenation signal and blood volume signal (in the unit of degree), thus it might also be larger than 90°.

3.2.2   *Image formation*

The images have been obtained by the back projection algorithm,[15] processed in MATLAB. In functional imaging, we take the difference between the rest state and activated state and then form the difference images, so the signals in the images will reflect the functional changes.

4   Experiment

4.1   Phantom Study

A number of experimental tests of the phased array system have been presented in previous articles.[14,16] Figure 4 shows an example of sharp amplitude null and phase transition with the displacement of an absorbing object (Black Delrin rod, 5 mm in diameter) along the X axis, with the steepest slope of phase transition up to 12°/mm.[17] A black object at a depth of

3 cm in an Intralipid+Ink background medium mimicking the human brain tissue ($\mu_a = 0.10$ cm^{-1}, $\mu_s' = 12$ cm^{-1}) can still be detected.

When the object is in the far left ($x \sim -6$ cm), the light beams from two sources (located at $x=\pm 2$ cm) are not affected by the object, so the detector fixed in the middle of two sources ($x=0$ cm) will detect the cancellation of two beams, i.e., amplitude is close to zero. As the object moves left, it blocks a larger proportion of light from left beam, so the photon density wave from the right source will predominate (note it is different from the situation shown in Figure 2). When the object is in the middle of the sources, it blocks two light beams equally, reaching an amplitude null again. This procedure can also be demonstrated qualitatively by vector diagrams proposed by Morgan et al.[18] A similar outcome to Figure 2 is that the amplitude curve is also symmetric to the middle plane of two sources, so in our later analysis, we focus our discussion more on the phase shift signals.

Figure 5 shows the two-dimensional back projection image (830 nm) of an absorbing object placed inside the scattering medium. The object is a black Delrin plastic cylinder with a diameter of 5 mm and a length of 10 mm, embedded inside the Intralipid with a depth of 2 cm. In the image we can locate the object, though the resolution is relatively low. We obtained similar images for 750 nm.

4.2   Blood Model Test

In the Intralipid+Ink medium with proper optical properties as human brain tissue ($\mu_a = 0.10$ cm^{-1}, $\mu_s' = 12$ cm^{-1}), a $4 \times 4 \times 8$ mm cellophane chamber is placed with 2.5 cm depth away from imager pad. The chamber is connected to a pump for oxygenated or deoxygenated blood. Filled with a certain concentration of blood (typically 8 mM), this chamber can be moved to various positions within the model. The perturbation of phase are plotted in Figure 6, which shows the difference between two wavelength signals, i.e., $|\Delta\Phi(830 \text{ nm})| - |\Delta\Phi(750 \text{ nm})|$. From Figure 6, the changes for oxygenated and deoxygenated blood are in opposite direction, and for black absorber, which has similar absorption coefficients for both wavelengths, shows almost zero signal after subtraction.

4.3   Functional Imaging for Neonates

4.3.1   *Method*

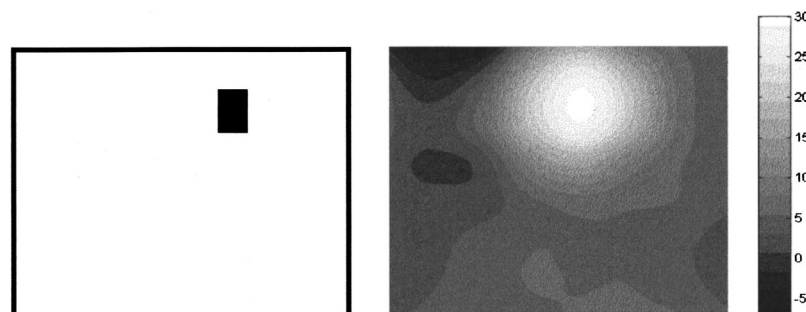We have studied seven neonates for a period of about two months, with the IRB approved informed consent from the

Fig. 5 Left: experimental geometry with the actual position of an absorbing object (black Delrin cylinder with diameter of 5 mm and length of 10 mm); Right: Two dimensional phase image of the object (830 nm).
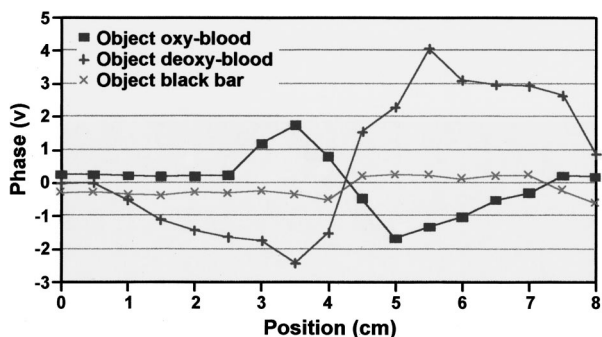
Fig. 6 (Signal 830–750 nm) Varies with displacement of absorber. Also note that the opposite trends for oxygenated blood and deoxygenated blood, and almost no change for neutral absorber (black delrin cylinder). (Phase is expressed in volt, which is proportional to phase angle in degree.)

Fig. 7 Placement of imager pad on neonate's head.

mothers of neonates. Six of the neonates are preterm (gestation: 27 ± 4 weeks) and their average age is 30 ± 18 days. Three of them have brain trauma (bleeding or epilepsy), while others are considered normal. The imager pad is placed on the middle region of neonates' head centered at *fonticulus* to cover the sensorimotor cortex, with a plastic wrap to prevent direct contact as shown in Figure 7. During the experiments, the neonates are stimulated by separately touching the four extremities and recording the signals in the contralateral sensorimotor cortex.

The experimental protocol is demonstrated below in Figure 8. The duration of each block is 30 s. The dark block indicates a resting state and the white block means functional testing. In the testing period, the doctor gently and continuously touches the infant's four extremities sequentially using swabs with equal intensity.

4.3.2   Results

A. Normal brain versus diseased brain: We have obtained the signals due to the blood volume and oxygenation changes caused by the sensory stimulation. Our results illustrate the difference in the response patterns and signal intensities of normal neonates and those who have diseased brain conditions. In normal neonates, we get reproducible responses. Figure 9(a) gives one example of the blood volume and oxygenation changes during a touching task. For subject *S*, a 33-wk gestational age infant with normal conditions, the signal changes occur in the region contralateral to the stimulus side. We observed the increases of blood volume and oxygenation saturation in the left side of the brain sensorimotor area during the stimulation. For instance, we stimulated the right foot of the neonate, and on the left part of the sensory area, we observed large responses (oxygenation image: $\Delta\Phi=60°$; blood volume image: $\Delta\Phi=90°$; total signal: $\Delta\Phi=150°$). The recovery of the signal is observed after 30 s of rest [oxygenation

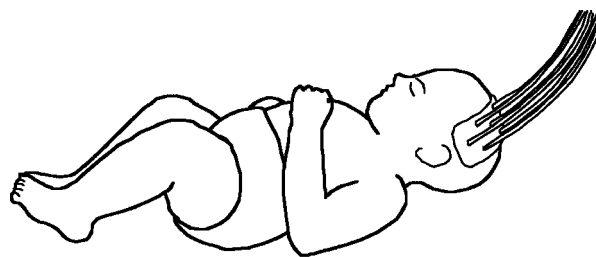image: $\Delta\Phi\sim5°$; blood volume image: $\Delta\Phi\sim10°$; see Figure 9(b)]. This can be interpreted as the sensory stimulation courses the increase in oxygen consumption, followed by an increase in blood flow.[19] The increase in blood flow provides more oxygen supply than the oxygen consumption so that an increase in oxygenation is observed. We did not observe the initial dip in oxygenation as described by Vanzetta and Grinvald,[20] which might be due to our long average time (16 s). In neonate with brain dysfunction, patient *N*, 27-wk gestational age with epilepsy, the signal is lower and nonlocalized [oxygenation image: $\Delta\Phi<5°$; blood volume image: $\Delta\Phi<5°$; see Figure 9(c)]. The image taken after 30 s recovery also has low signal intensity (not shown here).

The histogram for the total signals (|oxygenation signal| +|blood volume signal|) from all the imaging voxels (phased array channels) shows the different signal distribution for normal and diseased neonates (Figure 10). Figure 10(a) is the signal distribution for normal neonates and Figure 10(b) is the signal distribution for diseased neonates. It is obvious that the histogram is composed of background noise of the image, which has a Rayleigh distribution,[18,20] and the signal corresponding to stimulation, which is shown in the upper tail of the distribution (usually $>50°$). We can see that the normal neonates have a broader distribution of signal corresponding to stimulation (up to 160°) than that of diseased neonate (no signal larger than 100°).

Statistical analysis of the total signals from the responding voxels (not including the background) for normal and diseased populations with *t*-test shows there is a significant difference in the mean of total responding signals. (For normal subjects, mean and standard deviation$=109.5°\pm15.3°$; For abnormal subjects, mean and standard deviation$=26.1°\pm11.8°$; $P=0.004$. See Figure 11.)

B. Case study of cardiac arrest neonate: We have been able to study subject *W* (24-wk gestational age) over 21 days, postpartum. This subject had cardiac arrest for 30 min during delivery. Figures 12(a) and 12(b) show a large response to parietal stimulation and complete disappearance of the signal after 30 s rest period on the 1st day after resuscitation, which indicates the brain function was quite active. The 2nd day this
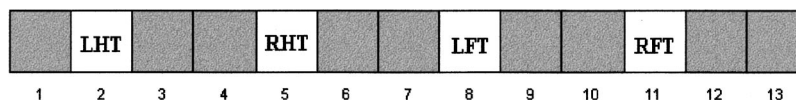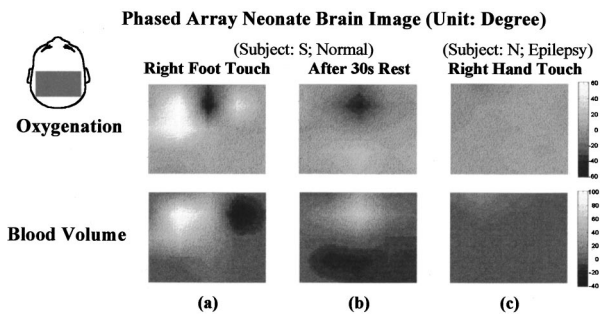

Fig. 8 Experiment protocol (LHT=left hand touch; RHT=right hand touch; LFT=left foot touch; RFT=right foot touch). Dark block means rest and bright block means functional test, each block lasts 30 s.

Phased Array Neonate Brain Image (Unit: Degree)

Fig. 9 Response to stimulation task from normal [(a) and (b)] and abnormal (c) subjects. (a) shows the signal corresponding to contralateral parietal stimulation; (b) shows the disappearance of signal 30 s after the stimulation ends; (c) for brain dysfunction neonate, no clear signal is observed. (For oxygenation images, "+" indicates oxygenation, and "−" indicates deoxygenation; for blood volume images, "+" indicates increase and "−" indicates decrease in blood volume.)

infant had a neonatal seizure, and no parietal response was observed on the tests on the following day (3rd day) [Figure 12(c)]. Then the infant gradually recovered and returned to functional condition. And the response to the stimulation can be observed again (images not shown here).

To examine the longitudinal tendency of the brain functional response, we plot the summation of phased array total signal intensity ($|$blood volume$| + |$oxygenation$|$) corresponding to all the four sensory stimulation in one day versus the test date in Figure 13. Here we observed summation of total
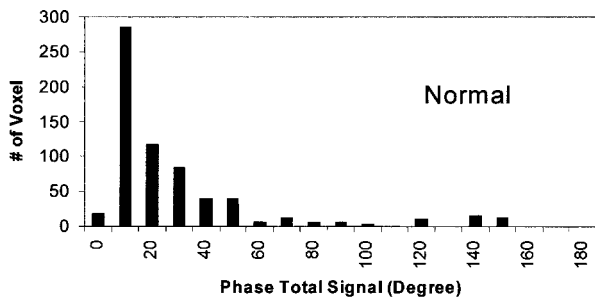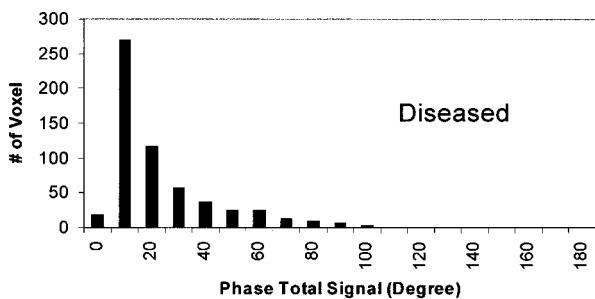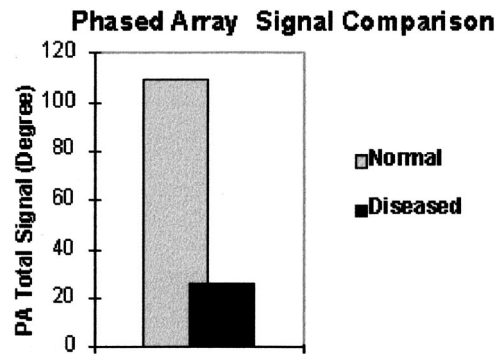

Fig. 10 (a) Histogram of the total signal in all the voxels from neonates in normal brain conditions; (b) Histogram of the total signal in all the voxels from neonates in diseased brain conditions. Note that there is signal distribution larger than 100° in (a) while there is none in (b).


Fig. 11 Statistical comparison of the mean of total signal from neonates in different brain conditions.
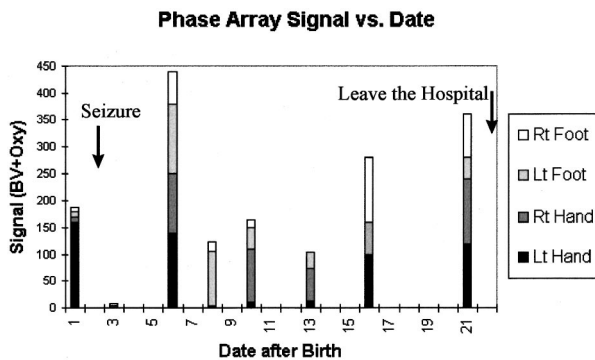
signal varied with the date after birth (resuscitation). On the first day after resuscitation, the neonate had partial response to the stimulation (strong response to left hand touch, while no obvious response to other stimulation), and the sum of total signal is 190°. After seizure, the neonate was inactive so that the sum of signal is only ~10° on date 3. On date 6 the infant seemed recovered and a little bit hypersensitive to the stimulation, and we got an overshooting in the sum of total signal (440°). Then the infant's condition fluctuated but remained at a certain level (date 8: 130°; date 10: 170°; date 13: 100°). Thereafter the neonate recovered gradually and got more sensitive to the stimulation (date 16: 280°; date 21: 360°). On date 21 the infant behaved normally and if we look at the average total signal for each stimulation, the result is roughly 90° (=360°/4), which is comparable to the mean of total signal for normal neonates we got in part A above (109.5°), considering the standard deviation is 15.3°. And on date 22, the infant totally recovered and left the hospital. The basic assumption here is the coupling between neuronal activation and the changes in local cerebral oxygenation and blood volume.[1] Thus the signal variance with date could be related to the neonate's brain condition.

5 Discussion

We have shown above that the two-wavelength phased array imaging system can successfully reveal the changes in blood concentration and oxygenation in functional brain activation for pre- and full-term neonates. Since this system is portable,
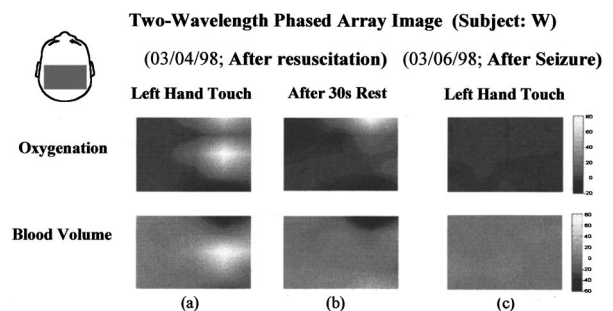
Fig. 12 Results of phased array imaging before and after seizure: response of stimulation (a) and disappearance of signal (b) after stimulation before seizure and no response (c) to parietal stimulation after seizure. (Image gray scale code same as Figure 8.)

Fig. 13 The summation of total signals from four stimulus on one day versus the date of testing (indicated by the date after birth and resuscitation), which shows the signal variation with different brain conditions. Note that there is almost no signal after the seizure (date 3) and the signal recovers gradually and finally reaches a normal value before the infant left the hospital (date 21).

it can be used for bedside monitoring and imaging of the infants neurological development and detecting the brain dysfunction.

There are also some difficulties in neonatal experiments. The spontaneous movement of the neonates is very hard to control during the experiment. When the neonate moves during stimulation, the response from movement (for example, kicking) will be strong enough to overwhelm the signal from sensory stimulation. A calm rest state as a good baseline is desirable. Also the recovery of the signal is a very important issue. For some tests, the recovery is very fast (within 30 s). However, in other cases, the recovery takes longer time (slow recovery), which will delay the response to the following test and make the signal smaller. The rate of recovery may also be related to neonatal brain condition, while further studies are needed to correlate it with clinical states.

Compared with other imaging modalities such as CT, MRI, and PET, optical imaging has relatively lower resolution. However this two-wavelength imaging technique has the capability of giving enhanced sensitivity of oxy- and deoxy-hemoglobin.[9] In addition, this system is portable and can be readily adapted for continuous monitoring, avoiding the transportation and immobilization of patients, especially pre- and full-term neonates.

Although the phased array imaging (PAI) system can sensitively detect the localized heterogeneity, it will be more helpful if combined with optical spectroscopic imaging technique such as phase modulation spectroscopic (PMS) imaging. Since PMS can be used to calculate the absolute absorption and scattering coefficients, the concentration of oxy- and deoxy-hemoglobin can be quantified. Such a combination will provide valuable information for medical evaluation and diagnosis.

Acknowledgments

References

1. A. Villringer and B. Chance, ''Noninvasive optical spectroscopy and imaging of human brain function,'' *Trends Neurosci.* **20**, 435–442 (1997).
2. F. F. Jobsis, ''Noninvasive infrared monitoring of cerebral and myocardial oxygen sufficiency and circulatory parameter,'' *Science* **198**, 1264–1267 (1977).
3. J. E. Brazy, D. V. Lewis, M. H. Mitnick, and F. F. Jobsis, ''Noninvasive monitoring of cerebral oxygenation in pre-term infants: Preliminary observations,'' *Pediatrics* **75**, 217–225 (1985).
4. B. Chance, Z. Zhuang, U. Chu, C. Alter, and L. Lipton, ''Cognition activated low frequency modulation of light absorption in human brain,'' *Proc. Natl. Acad. Sci. USA* **90**, 2660–2774 (1993).
5. Y. Hoshi, H. Onoe, Y. Wanatabe, J. Anderson, M. Bergstrom, A. Lilja, B. Langstom, and M. Tamura, ''Nonsynchronous behavior of neuronal activity, oxidative metabolism and blood supply during mental tasks in man,'' *Neurosci. Lett.* **172**, 129–133 (1994).
6. M. Cope and D. T. Delpy, ''System for the long-term measurement of cerebral blood and tissue oxygenation on newborn infants by near infrared transillumination,'' *Med. Biol. Eng. Comput.* **26**, 289–294 (1988).
7. B. Chance, Q. Luo, S. Nioka, D. C. Alsop, and J. A. Detre, ''Optical investigation of physiology: A study of biochemical intrinsic and extrinsic contrast,'' *Philos. Trans. R. Soc. London, Ser. B* **352**, 707–716 (1997).
8. S. R. Hintz, W.-F. Cheong, J. P. Van Houten, D. K. Stevenson, and D. A. Benaron, ''Bedside imaging of intracranial hemorrhage in the neonate using light: Comparison with Ultrasound, Computed Tomography, and Magnetic Resonance Imaging,'' *Pediatr. Res.* **45**, 54–59 (1999).
9. B. Chance et al., ''A novel method for fast imaging of brain function, non-invasively, with light,'' *Opt. Express* **2**, 411–423 (1998).
10. M. S. Patterson, B. Chance, and B. C. Wilson, ''Time resolved reflectance and transmittance for the non-invasive measurement of tissue optical properties,'' *Appl. Opt.* **28**, 2331–2336 (1989).
11. A. Yodh and B. Chance, ''Spectroscopy and imaging with diffusing light,'' *Phys. Today* **48**(3), 34–40 (1995).
12. J. B. Fishkin and E. Gratton, ''Propagation of photon-density waves in strongly scattering media containing an absorbing semi-infinite plane bounded by a straight edge,'' *J. Opt. Soc. Am. A* **10**, 127–140 (1993).
13. K. Kang, B. Chance, D. Bruley, and J. Londono, ''The application of near field interference of phase modulated spectroscopy for detection of absorbers: Theoretical prediction of phase shift with respect to the location of the absorber by using a probabilistic-numerical technique, the *B-W-K* method,'' *Proc. SPIE* **1888**, 340–353 (1993).
14. B. Chance, K. Kang, L. He, and S. Zhou, ''Precision localization of hidden absorbers in body tissues with phased-array optical systems,'' *Rev. Sci. Instrum.* **67**, 4324–4332 (1996).
15. S. Nioka, Y. Yang, M. Schnall, S. Zhao, S. Orel, C. Xie, B. Chance, and L. Solin, ''Optical imaging of breast tumor by means of continuous waves,'' in *Oxygen Transport to Tissue XVIII*, E. M. Nemoto, Ed., Plenum Publishing Corp., New York (1996).
16. B. Chance, K. Kang, L. He, J. Weng, and E. Sevick, ''Highly sensitive object location in tissue models with linear in-phase and antiphase multi-element optical arrays in one and two dimensions,'' *Proc. Natl. Acad. Sci. USA* **90**, 3423–3427 (1993).
17. B. Chance et al., ''Rapid and sensitive optical imaging of brain function,'' *OSA TOPS Adv. Opt. Imag. Photon Migration* **21**, 218–225 (1998).
18. S. Morgan, M. Somekh, and K. Hopcraft, ''Probabilistic method for phased array detection in scattering media,'' *Opt. Eng.* **37**, 1618–1626 (1998).
19. M. Henkelman, ''Measurement of signal intensities in the presence of noise in MR images,'' *Med. Phys.* **12**, 232–233 (1985).
20. I. Vanzetta and A. Grinvald, ''Increased cortical oxidative metabolism due to sensory stimulation: implications for functional brain imaging,'' *Science* **286**, 1555–1558 (1999).